Active Battery Cell Balancing by Real-Time Model Predictive Control for Extending Electric Vehicle Driving Range

Jun Chen[®], Senior Member, IEEE, Aman Behal[®], Senior Member, IEEE, Zhaojian Li, Senior Member, IEEE, and Chong Li, Senior Member, IEEE

Abstract- Electrical vehicles (EV) have been considered to be an effective way to combat global climate change. To extend the driving range of EV, this paper studies the active battery cell balancing control based on linear parametric varying model predictive control (MPC). Specifically, an equivalent circuit model is used to predict cell terminal voltage, and three different MPC-based battery cell balancing control strategies are proposed to dynamically transport electricity from cell to cell to reduce the imbalance. In particular, for the first control strategy, MPC is set up to be a tracking controller with the primary control objective of forcing all cells' terminal voltage to follow the same trajectory generated by a nominal cell model; for the second control strategy, MPC maximizes the lowest cell voltage, so that the battery operating range can be extended; for the third and last strategy, MPC minimizes the maximum variation among cell terminal voltages. To assess the effectiveness of the proposed battery cell balancing control strategies, simulations are performed on all three MPC formulations, using both steady-state and transient conditions. Numerical results show that the proposed battery cell balancing control can achieve a driving range extension of 9% for dynamic driving cycle and 7% for steady-state condition, based on our simulation setup. Compared to the existing work, our approaches do not require the over-restrictive assumption that the trip duration is known in advance, while at the same time achieve similar driving range extension. Furthermore, it is also shown that different driving condition favors different cell balancing control strategy, indicating a need for a hybrid approach. Finally, real time implementability is demonstrated via throughput analysis.

Manuscript received 8 February 2023; revised 15 May 2023; accepted 28 June 2023. Date of publication 10 July 2023; date of current version 8 August 2024. This article was recommended for publication by Associate Editor A. Parisio and Editor B. Vogel-Heuser upon evaluation of the reviewers' comments. This work was supported in part by the Faculty Startup Fund and Faculty Research Fellowship from Oakland University, in part by the Michigan Space Grant Consortium under Grant 80NSSC20M0124, and in part by the National Science Foundation under Award 2237317. (Corresponding author: Jun Chen.)

Jun Chen is with the Department of Electrical and Computer Engineering, Oakland University, Rochester, MI 48309 USA (e-mail: junchen@oakland.edu).

Aman Behal is with the Electrical and Computer Engineering and NanoScience Technology Center, University of Central Florida, Orlando, FL 32816 USA (e-mail: abehal@ucf.edu).

Zhaojian Li is with the Department of Mechanical Engineering, Michigan State University, East Lansing, MI 48824 USA (e-mail: lizhaoj1@msu.edu). Chong Li is with the Department of Electrical Engineering, Columbia University, NY 10027 USA (e-mail: cl3607@columbia.edu).

Color versions of one or more figures in this article are available at https://doi.org/10.1109/TASE.2023.3291679.

Digital Object Identifier 10.1109/TASE.2023.3291679

Note to Practitioners—Improving the efficiency of electric vehicles is of paramount importance to combat the global climate challenge. This paper contributes by proposing effective cell level balancing control methodologies to extend the driving range of electric vehicles to improve their energy efficiency and public acceptance. The control methods, which are based on model predictive control, are analytically derived with details for embedded implementation. Simulation results demonstrate the effectiveness of the proposed methodologies, with future work to investigate the applicability of nonlinear model predictive control with large number of cells.

Index Terms—Active battery cell balancing, electric vehicles, equivalent circuit model, model predictive control, quadratic programming.

I. Introduction

E LECTRIC vehicles are projected to make up 31% of the global fleet by 2050 [1] and have been considered to be a promising way to combat the global climate challenge by reducing over 3,000 kg carbon dioxide emission per vehicle per year [2]. Among many other choices, Lithium-Ion battery cells are dominating EV applications thanks to their high power and energy density [3], [4]. However, battery cells can suffer state-of-charge (SOC) and voltage imbalance, due to manufacturing and/or operation variations [5], [6]. Since the weakest cell determines the usable capacity of the whole battery pack, such imbalance would reduce EV driving range over single charge as well as life cycle, and result in safety issues such as thermal runaway [7], [8], [9], [10]. In order to increase EV driving range, battery cell balancing control has been proposed to reduce the variations among battery cells [11], [12], [13], [14], by using a balancing circuit [15], [16], [17], [18] such as flyback DC/DC converter [10], [15] and half-bridge converter [16], especially under conditions of higher power demand and high variation [17]. Battery cell balancing and can be either dissipative or nondissipative, where dissipative method removes charges from higher cells with higher SOC without reusing them [19] and nondissipative method transports electricity from cells to cells [10], [18]. Nondissipative battery cell balancing control can achieve greater energy saving benefit and higher efficiency, but at the same time requires sophisticated battery management systems to monitor and control the cell SOC/voltage. In this paper, we focus on nondissipative cell balancing control, which is also called active cell balancing and has less energy waste.

1545-5955 © 2023 IEEE. Personal use is permitted, but republication/redistribution requires IEEE permission. See https://www.ieee.org/publications/rights/index.html for more information.

The goal of active cell balancing is to push all cell's voltages away from a minimum bound, below which a cell would fail and lead to the failure of the entire battery pack. Several control techniques have been studied in the literature to achieve such goal [20], [21], [22], [23], [24], [25], such as simple feedback control [20], [21], rule-based control [22], [23], heuristic control [24], [25]. For example, [20] and [21] investigated simple feedback control, while rule-based control methods are utilized in [22] and [23]. In particular, reference [20] studied cell balancing problem and a simple feedback controller was utilized to calculate the balancing current in the context of renewable energy integration in the power grid, where heterogeneous battery systems with different types, ages, and rated capacity, were interconnected. The authors of [23] proposed a rule based balancing control algorithm for groupwise balancing and demonstrate the robustness and performance through realistic driving profile. In [22], a rulebased control strategy was adopted for cell balancing, where both voltage imbalance and SOC imbalance were considered in the criterion to trigger control action. Authors in [25] designed a power converter circuit that allows many to many balancing, and developed a fast simulation model for analysis. Heuristic strategy was developed and shows promising results in [24] and [25].

Though these aforementioned works [20], [21], [22], [23], [24], [25] demonstrate promising results, they rely on simple control method that do not fully utilize all electricity stored in battery cells. Towards this regard, model predictive control (MPC), a real-time receding horizon control technique [26], [27], [28], [29], [30], [31], [32], has been demonstrated to have great potential for active battery cell balancing control [8], [17], [18], [33], [34], [35], [36], [37], [38], [39]. For example, two linear MPC strategies were studied in [18], one optimizing charging and balancing simultaneously while the other using separate controls for charging and balancing. Software-in-theloop results and experiment validation were shown in [18] as well. Different balancing objectives, e.g., SOC, voltage, and charges, were considered in [8], which also adopted linear MPC method. Note that in [8], the MPC aims at tracking a reference trajectory generated by assuming the trip duration was known in advance. Though such an assumption was very restrictive, a 5% range increase was shown through simulation. The authors of [8] also demonstrated the robustness against the unknown driving cycle. To demonstrate the benefit of driving range extension, the authors of [7] cast the balancing control problem as a reachability analysis problem, which is computationally tractable for only a short driving cycle. References [36], [37], and [38] focused on nonlinear MPC. In particular, [36] considered both minimizing SOC variation and reducing energy waste in the nonlinear MPC formulation, with simulation results demonstrated on a two-cell battery. To reduce MPC computation for embedded implementation, reference [17] convexified of the control problem for the ease of computation, with significant problem simplification. Similarly, [33] utilized fast MPC, where the optimal control problem was reformulated into a linear programming problem, suitable for an embedded environment. Finally, distributed control has also been studied in literature for battery control [40], [41], [42], [43], [44]. Specifically, distributed MPC control strategies for active battery cell balancing was studied in [42], where cells are grouped into submodules and then modules. The higher level control optimizes modules balancing current by assuming a certain parameterization on the intramodule currents, with the lower level control optimizing the balancing currents within each module. Distributed control strategy with module topology constraints were applied for SOC balancing between the battery modules of a reconfigurable battery energy storage system in [40]. Though the proposed work in [40] was applied to generic battery balancing problem, the approach can be extended to EV applications.

However, there are several limitations with the aforementioned MPC-based active battery cell balancing. For example, only tracking controller was considered in [8], [36], and [42], which *indirectly* achieves the goal of pushing all cell voltages away from the minimum bound. Moreover, the assumption in [8] that the trip duration is known in advance for reference generation, can be very restrictive given the current technology and make the developed control algorithm not practical for short-term deployment. Furthermore, most of the work either utilize linear prediction model [8], [17], [18] that can result in over simplification or nonlinear model [36], [37], [38] that cause high computation cost, and a better approach that intermingle these two, e.g., linear parametric varying (LPV) prediction model, is needed.

To address these limitations, In this paper, we study LPV MPC for active battery cell balancing problem for EV driving range extension, and investigate three different balancing control strategies. For the first control strategy, MPC is set up to be a tracking controller with the primary control objective of forcing all cells' terminal voltage to follow the same short-term trajectory generated by a nominal cell model. This setup is similar to the MPC formulation of [8], without assuming that the trip duration is known in advance. For the second control strategy, MPC maximizes the lowest cell voltage, so that the battery operating range can be extended. Finally, for the third strategy, MPC minimizes the maximum variation among cell terminal voltages. Note that the eventual control objective here is to push all cell's voltages away from the minimum bound, below which a cell would fail and lead to the failure of the entire battery pack. The three proposed MPC control strategies achieve this goal by using different cost functions, whose effectiveness are assessed through simulations with both steady-state and transient conditions. Numerical results show that the proposed battery cell balancing control can achieve a driving range extension of 9% for dynamic driving cycle and 7% for steady-state condition. Furthermore, it is also shown that different driving condition favors different cell balancing control strategy, indicating a need for a hybrid approach. Finally, real time implementability is demonstrated via throughput analysis.

Comparing to the existing work, our contribution are summarized below.

 Our approaches do not require the over-restrictive assumption that the trip duration is known in advance, while at the same time achieve similar driving range extension.

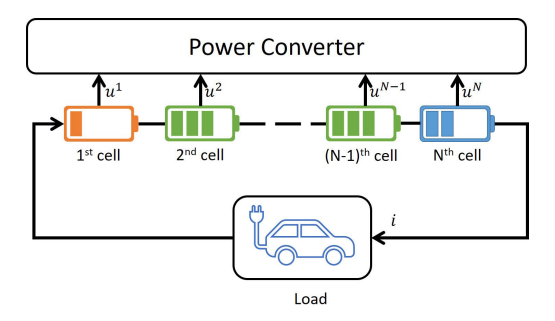


Fig. 1. Structure of series connected battery cells with balancing current.

- The proposed MPC strategies allow direct maximization of the lowest cell voltage, instead of indirectly achieving this goal through tracking controller.
- The proposed MPC formulations can be cast into linearly constrained quadratic programming problem, which has been proven to be suitable for real-time implementation.
- 4) Extensive simulations using both steady-state and transident driving profiles are performed to evaluate the effectiveness of the proposed active battery balancing control strategies and demonstrate the EV driving range extension.

A preliminary version of this work [45] has been presented in 2021 IEEE Conference on Decision and Control. This submitted manuscript extends the conference version by completing literature review, including details on control design, correcting several oversights, improving the simulation environment, and supplementing with additional results and analysis. All results in the submitted manuscript are updated. The rest of this paper is organized as follows. Section II presents the equivalent circuit model for each cell and the whole battery pack, while Section III formulates the optimal control problems and three MPC setups. Section IV presents numerical results, and the paper is concluded in Section V.

II. ACTIVE CELL BALANCING

The series connected battery considered here is shown in Fig. 1, where N cells are stacked to provide the requested current i to the load, e.g. an EV in this case. Note that we only consider series connection here for the simplicity of presentation. The proposed control methodologies and corresponding analysis can be straightforwardly extended to the case with parallel connections. Note that the request of current i can be made, for example, from higher level controller. Note that different power converters can result in different balancing performances. In this work, we ignore the dynamic of the power converter and proposed a generic framework for MPC-based active cell balancing control. The development of MPC that explicitly incorporate the dynamic of power converter will remain a future work direction.

Recall that EV battery pack usually consists of hundreds of cells, and the SOC and voltage of each cell can be significantly different from each other due to manufacturing variation and/or different aging conditions. When the voltage of the weakest cell drops below a certain minimum bound, denoted

as v_{\min} , the whole battery pack stops operation due to safety reason. Therefore, the control objective of active battery cell balancing is then to dynamically relocate electric charges from cell to cell, through a power converter circuit, so that all the voltages of all cells stay away from the minimum bound v_{\min} . In other words, the goal is to find the balancing current u_k^n for each cell $n=1,\ldots,N$ and for each time step $k=0,1,\ldots$, so that the cell voltage v_k^n satisfies

$$v_{\min} \le v_k^n. \quad n = 1, \dots, N \quad \& \quad \forall k, \tag{1}$$

for any driving cycle in the form of power profile P_k or current profile i_k . Note that the problem formulation considered here is similar to the one investigated in [8]. However, as will be seen shortly, we propose completely solution approaches compared to [8].

Note that u_k for all time steps k cannot be determined at the same time, since in practice we do not have the entire driving cycle P_k . Furthermore, solving u_k for all k together requires significant computational power that makes it impractical for real-time application. Fortunately, this problem can be reformulated into receding horizon control problem. In particular, we adopt model predictive control (MPC) method, which uses a relatively short horizon p to predict the future evolution and optimizes a certain objective function over this prediction horizon. In other words, we usually have $p \ll N$. At each time step, a control sequence over the entire prediction horizon is obtained, but only the first element is implemented. At next time step, the whole process repeats. Denoting $u_k = \begin{bmatrix} u_k^1, u_k^2, \ldots, u_k^N \end{bmatrix}^T$, the optimal control problem (OCP) for MPC to solve at time k is given by

$$\min_{u_k} J(u_k) \tag{2a}$$

$$u_{\min} \le u_k^n \le u_{\max}, \quad n = 1, \dots, N$$
 (2c)

$$v_{\min} \le y_{k+j}^n, \quad j = 1, \dots, p, \ n = 1, \dots, N$$
 (2d)

$$0 = \sum_{n=1}^{N} u_k^n, \tag{2e}$$

where $J(u_k)$ is a cost function to be formally defined in Section IV. See Section III for more details regarding the linearized battery model development. The last constraint (2e) indicates that the balancing circuit is only responsible to transport charge from one cell to another, and cannot provide or consume any additional charge (hence different from dissipative balancing strategy where the summation of all balancing current can be positive).

Remark 1: Note that in OCP (2), the MPC is to optimize one balancing current u_k^n for each cell, which is then kept unchanged over the entire prediction horizon. In other words, we do not calculate u_{k+j}^n for $j=0,\ldots,p-1$, and instead set $u_{k+j}^n=u_k^n$ throughout the prediction horizon. This strategy is adopted from [8] as the balancing currents are almost constant over the prediction horizon. Such an arrangement can significantly reduce the size of the OCP for real-time implementation.

Remark 2: Note that though we consider constant minimum bound v_{\min} in (2d) for our numerical study, the OCP (2) can

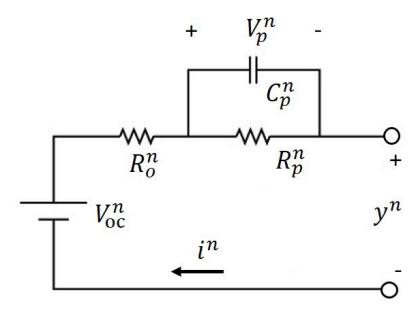


Fig. 2. Equivalent circuit model of a battery cell.

be straightforwardly extended to include the case when the minimum allowable voltage is changing dynamically. In other words, the value of v_{\min} can be changed dynamically to accommodate transient condition. In this case, a new value for $v_{\min,k}$ needs to be computed and received by MPC for each sampling time k.

III. BATTERY MODEL

The OCP (2) requires a linearized battery model to predict the system evolution over the prediction horizon. This section briefly reviews the nonlinear battery model, and later linearize it for MPC.

A. Equivalent Circuit Model

The dynamics of each battery cell can be modeled using an equivalent circuit model (ECM), which provides a good balance between accuracy and computational cost. Note that ECM has been widely used in the literature to study the dynamic behavior of Li-Ion battery [46], [47], [48], [49], [50], [51], [52]. Specifically, second order ECM has been used in literature for cell balancing control due to the simplicity to model and ease of computation. See for example [8] and [7]. In this section, we briefly describe second order ECM as follows. For more details, please refer to the aforementioned references and the references therein.

The ECM used to model a battery cell is shown in Fig. 2, where the superscript n denotes the nth cell, V_{oc}^n is the open circuit voltage, v^n is the terminal voltage, R_o^n , R_p^n , and C_p^n are resistance and capacitor of the ECM, respectively, and i^n is the battery pack current. We use the convention that positive value of i^n indicates discharging from the battery cell and negative indicates charging to the battery cell. Denote s^n as the remaining SOC of cell n. The cell dynamics are then specified by

$$\dot{s^n} = -\eta^n \frac{i^n}{3600C^n} \tag{3a}$$

$$\dot{s^n} = -\eta^n \frac{i^n}{3600C^n}$$
(3a)
$$\dot{V_p^n} = -\frac{V_p^n}{R_p^n C_p^n} + \frac{i^n}{C_p^n}$$
(3b)

$$v^n = V_{oc}^n - V_p^n - i^n R_o^n, (3c)$$

where η^n is the coulombic efficiency of cell n, C^n is the cell Amp-Hour capacity, and V_p^n is the relaxation voltage over the RC component. Note that V_{oc}^n , R_o^n , R_p^n , and C_p^n are all

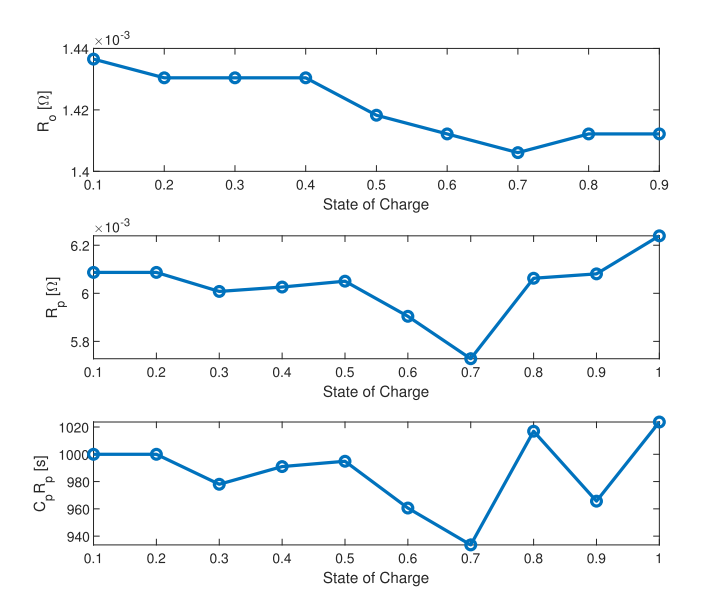


Fig. 3. Parameters for a nominal cell, adopted from [49].

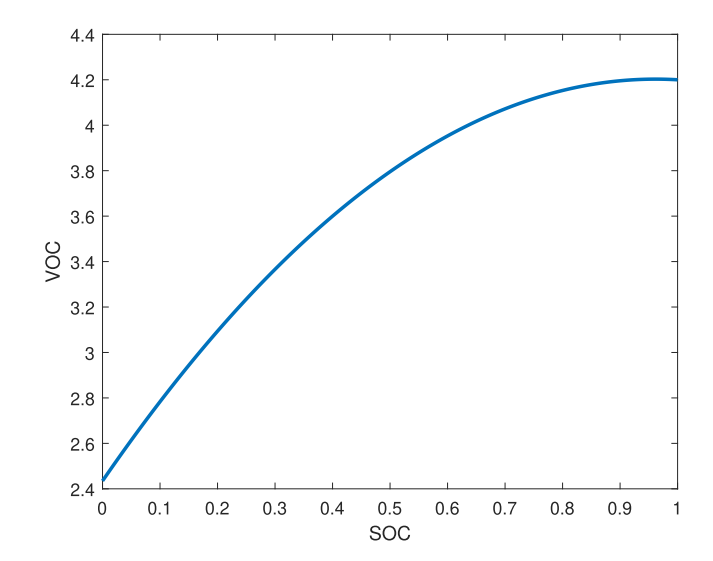


Fig. 4. Open circuit voltage versus state of charge.

dependent on s^n , making (3) a nonlinear model, i.e., nonlinear with respect to states. Fig. 3 depicts an example of such dependency for R_o^n , R_p^n , and C_p^n for a nominal cell, as adopted from [49]. Furthermore, $V_{oc}^n = -1.9123(s^n)^2 + 3.6775(s^n) +$ 2.4348. (See Fig. 4.) Note that due to manufacturing variation and/or different aging conditions, the dependency of V_{oc}^n , R_o^n , R_p^n , and C_p^n on s^n can be different for each cell n, resulting different characteristics for each cell.

Denote $x^n := [s^n, V_p]^T$ where \cdot^T denotes matrix/vector transpose, then one can write (3) as

$$\dot{x^n} = f^n(x^n, i^n), \qquad v^n = g^n(x^n, i^n),$$
 (4a)

where functions $f^n(x, i^n)$ and $g^n(x, i^n)$ are defined by (3). Considering the battery structure in Fig. 1, the current i^n drawn through cell n equals the pack current i plus balancing current u^n . Therefore, we can rewrite (4) as

$$\dot{x^n} = f^n(x^n, i + u^n), \qquad v^n = g^n(x^n, i + u^n).$$
 (5a)

Define $x = [x^1, x^2, ..., x^N]^T$ as the state vector for the entire battery pack and v_b as the terminal voltage of the battery pack, then we have

$$\dot{x} = \begin{bmatrix} f^{n}(x^{1}, i + u^{1}) \\ f^{n}(x^{2}, i + u^{2}) \\ \vdots \\ f^{n}(x^{N}, i + u^{N}) \end{bmatrix}$$
 (6a)

$$v_{b} = \sum_{n=1}^{N} v^{n} = \sum_{n=1}^{N} g^{n}(x^{n}, i + u^{n}).$$
 (6b)

which will be used as the virtual plant for simulation study as well as the prediction model for MPC after online linearization and discretization. See Section III-B.

B. Model Linearization and Discretization

To derive a linearized discrete-time prediction model for MPC, denote for cell n its the current state estimate and output as $\hat{x}_k^n = [\hat{s}_k^n; \hat{V}_{p,k}^n]$ and \hat{v}_k^n , where k denotes the current time step. Furthermore, denote \hat{u}_k^n and \hat{i}_k as the nominal balancing current and pack current, respectively, for time k. In this study, we simply choose the balancing current applied at previous control loop as \hat{u}_k^n and the requested pack current at time k as \hat{i}_k . Further denote $\delta x_k^n = [\delta s_k^n; \delta V_{p,k}^n], \delta v_k^n, \delta i_k$ and δu_k^n as the deviations from their nominal values. Then, Equ. (5) can be linearized as follows.

$$\begin{split} \delta \dot{s}_{k}^{n} &= -\eta^{n} \frac{\hat{i}_{k} + \hat{u}_{k}^{n}}{C^{n}} - \eta^{n} \frac{1}{C^{n}} \delta i_{k} - \eta^{n} \frac{1}{C^{n}(\hat{s}_{k}^{n})} \delta u_{k}^{n} \\ \delta \dot{V}_{p,k}^{n} &= -\frac{\hat{V}_{p,k}^{n}}{R_{p}^{n}(\hat{s}_{k}^{n}) C_{p}^{n}(\hat{s}_{k}^{n})} + \frac{\hat{i}_{k} + \hat{u}_{k}^{n}}{C_{p}^{n}(\hat{s}_{k}^{n})} \\ &+ \frac{\hat{V}_{p,k}^{n}}{\left(R_{p}^{n}(\hat{s}_{k}^{n}) C_{p}^{n}(\hat{s}_{k}^{n})\right)^{2}} \frac{\partial \left(R_{p}^{n}(s^{n}) C_{p}^{n}(s^{n})\right)}{\partial s^{n}} \bigg|_{s^{n} = \hat{s}_{k}^{n}} \delta s_{k}^{n} \\ &- \frac{\hat{i}_{k} + \hat{u}_{k}^{n}}{\left(C_{p}^{n}(\hat{s}_{k}^{n})\right)^{2}} \frac{\partial C_{p}^{n}(s^{n})}{\partial s^{n}} \bigg|_{s^{n} = \hat{s}_{k}^{n}} \delta s_{k}^{n} \\ &- \frac{1}{R_{p}^{n}(\hat{s}_{k}^{n}) C_{p}^{n}(\hat{s}_{k}^{n})} \delta V_{p,k}^{n} + \frac{1}{C_{p}^{n}(\hat{s}_{k}^{n})} \delta i_{k} + \frac{1}{C_{p}^{n}(\hat{s}_{k}^{n})} \delta u_{k}^{n} \\ v_{k}^{n} &= V_{oc}^{n}(\hat{s}_{k}^{n}) - \hat{V}_{p,k}^{n} - \hat{i}_{k} R_{o}^{n}(\hat{s}_{k}^{n}) + \frac{\partial V_{oc}^{n}(s^{n})}{\partial s^{n}} \bigg|_{s^{n} = \hat{s}_{k}^{n}} \delta s_{k}^{n} \\ &- (\hat{i}_{k} + \hat{u}_{k}^{n}) \frac{\partial R_{o}^{n}(s^{n})}{\partial s^{n}} \bigg|_{s^{n} = \hat{s}_{k}^{n}} \delta s_{k}^{n} \\ &- \delta V_{p,k}^{n} - R_{o}^{n}(\hat{s}_{k}^{n}) \delta i_{k} - R_{o}^{n}(\hat{s}_{k}^{n}) \delta u_{k}^{n}. \end{split}$$

Putting everything together, we have

$$\begin{aligned}
\delta \dot{x}_{k}^{n} &= f^{n}(\hat{x}_{k}^{n}, \hat{i}_{k} + \hat{u}_{k}^{n}) + A_{k}^{c} \delta x_{k}^{n} + B_{k}^{c} \delta u_{k}^{n} + B_{d,k}^{c} \delta i_{k} \\
v_{k}^{n} &= g^{n}(\hat{x}_{k}^{n}, \hat{i}_{k} + \hat{u}_{k}^{n}) + C_{k}^{c} \delta x_{k}^{n} + D_{k}^{c} u_{k}^{n} + D_{d,k}^{c} \delta i_{k}, \quad (7b)
\end{aligned}$$

where A_k^c is a 2 × 2 matrix, B_k^c and $B_{d,k}^c$ are 2 × 1 matrices, C_k^c is a 2 × 2 matrix, D_k^c and $D_{d,k}^c$ are scalar, with elements

specified as follows.

$$\begin{split} A_{k}^{c}(1,1) &= 0, \quad A_{k}^{c}(1,2) = 0 \\ A_{k}^{c}(2,1) &= \frac{\hat{V}_{p,k}^{n}}{\left(R_{p}^{n}(\hat{s}_{k}^{n})C_{p}^{n}(\hat{s}_{k}^{n})\right)^{2}} \frac{\partial \left(R_{p}^{n}(s^{n})C_{p}^{n}(s^{n})\right)}{\partial s^{n}} \bigg|_{s^{n} = \hat{s}_{k}^{n}} \\ &- \frac{\hat{i}_{k} + \hat{u}_{k}^{n}}{\left(C_{p}^{n}(\hat{s}_{k}^{n})\right)^{2}} \frac{\partial C_{p}^{n}(s^{n})}{\partial s^{n}} \bigg|_{s^{n} = \hat{s}_{k}^{n}} \\ A_{k}^{c}(2,2) &= -\frac{1}{R_{p}^{n}(\hat{s}_{k}^{n})C_{p}^{n}(\hat{s}_{k}^{n})} \\ B_{k}^{c} &= B_{d,k}^{c} = \left[-\eta^{n} \frac{1}{C_{n}^{n}(\hat{s}_{k}^{n})} \frac{1}{C_{p}^{n}(\hat{s}_{k}^{n})} \right]^{T} \\ C_{k}^{c}(1,1) &= \frac{\partial V_{oc}^{n}(s^{n})}{\partial s^{n}} \bigg|_{s^{n} = \hat{s}_{k}^{n}} - (\hat{i}_{k} + \hat{u}_{k}^{n}) \frac{\partial R_{o}^{n}(s^{n})}{\partial s^{n}} \bigg|_{s^{n} = \hat{s}_{k}^{n}} \\ C_{k}^{c}(1,2) &= -1, \quad D_{k}^{c} &= -R_{p}^{n}(\hat{s}_{k}^{n}), \quad D_{d,k}^{c} &= D_{k}^{c}. \end{split}$$

The linearized model (7) can be further discretized using Euler's forward integration as follows, where T_s denotes the sampling.

$$\delta x_{k+1}^n = \hat{f}_k^n + A_k \delta x_k^n + B_k \delta u_k^n + B_{d,k} \delta i_k \tag{8a}$$

$$v_k^n = \hat{g}_k^n + C_k \delta x_k^n + D_k u_k^n + D_{d,k} \delta i_k, \tag{8b}$$

where

$$\hat{f}_{k}^{n} = f^{n}(\hat{x}_{k}^{n}, \hat{i}_{k} + \hat{u}_{k}^{n})T_{s} \tag{9a}$$

$$A_k = I + A_k^c T_s \tag{9b}$$

$$B_k = B_k^c T_s \tag{9c}$$

$$B_{d,k} = B_k \tag{9d}$$

$$\hat{g}_{k}^{n} = g^{n}(\hat{x}_{k}^{n}, \hat{i}_{k} + \hat{u}_{k}^{n})$$
 (9e)

$$C_k = C_k^c \tag{9f}$$

$$D_k = D_k^c \tag{9g}$$

$$D_{dk} = D_k \tag{9h}$$

Remark 3: Note that this linearized model is parametric varying, since at each time step k, a new set of matrices are obtained based on the current operating conditions \hat{x}_k^n , \hat{v}_k^n , \hat{u}_k^n , and \hat{i}_k . Furthermore, (8) is scheduled according to SOC s, which is often not measured. However, several techniques in literature that can effectively estimate s according to terminal voltage measurement. See for example [23], [36], [40], [42], [49], and [53].

Remark 4: Note also that the since the linearized model above requires a nominal operating battery pack current \hat{i}_k , which can be time varying over the prediction horizon of the OCP (2). Therefore, the active battery balancing control based on OCP (2) would require a short-term prediction of the load profile over the prediction horizon, i.e., i_{k+j} for $j=1,\ldots,p$. Such preview can often be available from high level controller such as vehicle speed control unit. However, when such preview is not available, the value at time k can be used throughout the whole horizon, i.e., $i_{k+j}=i_k$ for $j=1,\ldots,p$.

IV. CONTROL STRATEGIES

In this section, we present three different control strategies to perform the active battery cell balancing to extend EV driving range. Recall that the goal of active cell balancing is to push all cell's voltages away from a minimum bound, below which a cell would fail and lead to the failure of the entire battery pack. To achieve this goal, we propose and evaluate three MPC-based control strategies to dynamically transport electricity from cell to cell to reduce the imbalance. For the first control strategy, MPC is set up to be a tracking controller with the primary control objective of forcing all cells' terminal voltage to follow the same short-term trajectory generated by a nominal cell model. This setup is similar to the MPC formulation of [8], without assuming that the trip duration is known in advance. For the second control strategy, MPC maximizes the lowest cell voltage, so that the battery operating range can be extended. Finally, for the third strategy, MPC minimizes the maximum variation among cell terminal voltages.

A. Tracking-Based Balancing Control

In the first formulation, we use a nominal cell model to integrate over the prediction horizon based on the requested total current i_k (or i_{k+j} if preview is available), and the resulting voltage trajectory is used as reference that all cells need to track. More specifically, the dynamics of the nominal cell are the same as those of (3) but with nominal parameters, as shown in Fig. 3. Then we integrate the nominal cell model using the initial condition $x_k^0 = \frac{1}{N} \sum_{n=1}^N x_k^n$ to obtain the reference sequences $x_{k+1}^0, x_{k+2}^0, \ldots, x_{k+p}^0$ and $v_{k+1}^0, v_{k+2}^0, \ldots, v_{k+p}^0$. Further define the reference voltage as

$$v_{k+j}^r = \underbrace{\left[v_{k+j}^0, \ v_{k+j}^0, \ \dots, \ v_{k+j}^0\right]^T}_{N \text{ blocks}}$$

Then the OCP for tracking-based balancing control can be represented as

$$\min_{u_k} \sum_{i=1}^{p} (v_{k+j} - v_{k+j}^r)^T (v_{k+j} - v_{k+j}^r) + u_k^T R u_k, \quad (10a)$$

$$u_{\min} \le u_k^n \le u_{\max}, \quad n = 1, \dots, N \tag{10c}$$

$$v_{\min} \le y_{k+j}^n, \quad j = 1, \dots, p, \ n = 1, \dots, N$$
 (10d)

$$0 = \sum_{n=1}^{N} u_k^n, \tag{10e}$$

where the cost function (10a) is denoted as J_t with R is a positive definitive weighting matrix.

Remark 5: Note that the first term of (10a) is to track all cell voltage to follow the reference trajectory v_{k+j}^r , while the second term penalizes large balancing currents to reduce energy waste, which results from resistant heating. Note also that we only impose weighting matrix in the second term. This is because all the cell terminal voltages have the same scale, and the balance between voltage tracking and control efforts can be achieved through the R matrix alone.

Remark 6: In this work, the initial condition for integrating the nominal cell is given by averaging all cells' state vectors. Another approach to obtain the initial condition is to utilize an observer to estimate the state of the nominal cell based

on measurement from battery pack. This however remains as future work.

Remark 7: MPC strategy based on OCP (10) is similar to the MPC formulation of [8]. However, the way that the reference trajectory is generated in our work does not assume that the trip duration is known in advance, which can be a restrictive assumption in reality.

B. Max-Min Balancing Control

The control strategy of (10) is intuitive to understand. However, forcing all cells to follow the same reference trajectory can sometimes be too aggressive, especially considering that the primary goal of balancing control is to ensure the lowest cell voltage stay away from the minimum bound. Therefore, we propose the second formulation which, instead of tracking a nominal trajectory, directly maximizes the lowest cell voltage. In other words, the OCP is defined as follows.

$$\min_{u_k} - \sum_{j=1}^p \min_n v_{k+j}^n + u_k^T R u_k,$$
 (11a)

$$u_{\min} \le u_k^n \le u_{\max}, \quad n = 1, \dots, N \tag{11c}$$

$$v_{\min} \leq y_{k+j}^n, \quad j = 1, \dots, p, \ n = 1, \dots, N$$
 (11d)

$$0 = \sum_{n=1}^{N} u_k^n, \tag{11e}$$

where the cost function (11a) is denoted as $J_{\rm m}$ with R is a positive definitive weighting matrix. Note that the OCP (11) aims to *maximize* the lowest cell voltage for each time step over the prediction horizon with minimum balancing current.

To reformulate (11) for embedded environment, the trick discussed in [54] is adopted as follows. Define p slack variables as $\epsilon = [\epsilon_1, \epsilon_2, \ldots, \epsilon_p]^T$. Then the objective function (11a) can be rewritten as,

$$J_{\mathrm{m}}(u_k,\epsilon) = -\sum_{i=1}^{p} \epsilon_j + u_k^T R u_k,$$

with additional constraint

$$\epsilon_j \leq v_{k+j}^n, j = 1, \dots, p, \quad n = 1, \dots, N.$$

Please refer to [54] for more details. In other words, the max-min balancing control solves the following OCP at every time step.

$$\min_{u_k,,\epsilon} -\sum_{i=1}^p \epsilon_j + u_k^T R u_k, \tag{12a}$$

$$\epsilon_j \le v_{k+j}^n, \qquad j = 1, \dots, p, \quad n = 1, \dots, N \quad (12c)$$

$$u_{\min} \le u_k^n \le u_{\max}, \quad n = 1, \dots, N \tag{12d}$$

$$v_{\min} \le y_{k+j}^n, \quad j = 1, \dots, p, \ n = 1, \dots, N$$
 (12e)

$$0 = \sum_{k=1}^{N} u_k^n, \tag{12f}$$

C. Minimum Bound Balancing Control

Finally, in the third (and last) control strategy, instead of maximizing the lowest cell voltage, MPC is set up to minimize the difference between the highest and lowest cell voltage. The primary goal of this approach is to encourage MPC to directly move electric charges from cell with highest voltage. More specifically, the OCP in this case is defined as follows.

$$\min_{u_k} \sum_{j=1}^{p} \left(\max_{n} v_{k+j}^n - \min_{n} v_{k+j}^n \right) + u_k^T R u_k,$$
 (13a)

$$u_{\min} \le u_k^n \le u_{\max}, \quad n = 1, \dots, N$$
 (13c)

$$v_{\min} \le v_{k+j}^n, \quad j = 1, \dots, p, \ n = 1, \dots, N$$
 (13d)

$$0 = \sum_{n=1}^{N} u_k^n, \tag{13e}$$

where the cost function (13a) is denoted as J_{Δ} and R is a positive definite weighting matrix. Note that the OCP (13) aims to minimize the cell voltage variation by reducing the bound of the difference of the cell voltages.

To reformulate (13) for embedded environment, define 2p slack variables as, with a slight abuse of notation, $\epsilon = [\epsilon_1, \epsilon_2, \ldots, \epsilon_p, \epsilon_{p+1}, \ldots, \epsilon_{2p}]^T$. Then the objective function (13a) can be rewritten as,

$$J_{\Delta,\sigma}(u_k, \epsilon) = \sum_{j=1}^{p} \left(\max_{n} \sigma_{k+j}^n - \min_{n} \sigma_{k+j}^n \right) + u_k^T R u_k$$

$$= \sum_{j=1}^{p} \max_{n} \sigma_{k+j}^n - \sum_{n=1}^{p} \min_{n} \sigma_{k+j}^n + u_k^T R u_k$$

$$= \sum_{j=1}^{p} \epsilon_{p+j} - \sum_{j=1}^{p} \epsilon_j + u_k^T R u_k,$$

with additional constraint

$$\epsilon_j \leq \sigma_{k+j}^n, j = 1, \dots, p, \quad n = 1, \dots, N$$

 $\epsilon_{p+j} \geq \sigma_{k+j}^n, j = 1, \dots, p, \quad n = 1, \dots, N.$

In other words, the minimum bound balancing control solves the following OCP at every time step.

$$\min_{u_k,\epsilon} \sum_{j=1}^p \epsilon_{p+j} - \sum_{j=1}^p \epsilon_j + u_k^T R u_k$$
 (14a)

$$\epsilon_j \le \sigma_{k+j}^n, \quad j = 1, \dots, p, \ n = 1, \dots, N$$
 (14c)

$$\epsilon_{p+j} \ge \sigma_{k+j}^n, \quad j = 1, \dots, p, \ n = 1, \dots, N,$$
 (14d)

$$u_{\min} \le u_k^n \le u_{\max}, \quad n = 1, \dots, N$$
 (14e)

$$v_{\min} \le y_{k+j}^n, \quad j = 1, \dots, p, \ n = 1, \dots, N$$
 (14f)

$$0 = \sum_{n=1}^{N} u_k^n, \tag{14g}$$

Remark 8: Please note that different from [54], constraints in (12c), (14c), and (14d) are only one sided, e.g., $\epsilon_j \leq \sigma_{k+j}^n$ instead of $\epsilon_j \leq \pm \sigma_{k+j}^n$. This is because v^n is positive by design

and hence the complexity of the resulting OCP (12) and (14) are slightly reduced.

Remark 9: Please note that all three MPC formulations, namely (10), (12) and (14) can all be cast into quadratic programming (QP) problem, which can be solved in real time by embedded devices when the problem size is manageable [55], [56], [57]. Assuming sparse QP formulation, J_t then has (2p+1)N optimization variables, J_m has (2p+1)N+p optimization variables with additional pN constraints, while J_{Δ} has (2p+1)N+2p optimization variables with additional 2pN constraints. Therefore, J_m and J_{Δ} have larger problem sizes and require larger amount of computation to solve, while at the same time, provide certain benefits in some conditions, as will be seen in the next section.

Remark 10: Note that the output constraints (10d), (12e), and (14f) can be infeasible when the cell voltage is approaching the minimum bound v_{\min} . In other words, when the lowest cell voltage is close to v_{\min} , no matter what balancing current u_k MPC chooses, the constraints (10d), (12e), and (14f) are going to be violated over the prediction horizon. However, in this case, we still want MPC to compute a control input so that such constraints violation are minimized. To do that, we introduce an additional slack variable ϵ_v , and add to each cost function an additional term $W\epsilon_y^2$ where $W\gg R$. Furthermore, (10d), (12e), and (14f) are modified as follows,

$$v_{\min} \le v_{k+j}^n + \epsilon_y, \qquad j = 1, \dots, p, \ n = 1, \dots, N.$$
 (15)

In other words, MPC will initially solve the original OCP (10), (12), (14), and when the OCP is found to be infeasible (which usually occurs towards the end of driving cycle), MPC will then modify the cost function and replace (10d), (12e), or (14f) with (15) as discussed here. Note that this is called "soft constraint" in literature, and has been applied to avoid infeasible OCP [55], [56].

V. NUMERICAL RESULTS

In this section, several simulations are performed to demonstrate the effectiveness of the proposed MPC-based active battery cell balancing control strategies. Specifically, the linearized parametric model (8) will be used by MPC to form the OCPs, and the original nonlinear model (3) with SOC-dependent parameters and additive process noise will be used as simulation plant to mimic model mismatch. Furthermore, two scenarios are considered. In the first scenario, a constant requested current i_k is considered, which is selected so that the simulation can be conducted in a reasonable amount of time. In the second scenario, the vehicle follows a realistic driving cycle, i.e., FTP cycle, where the vehicle is controlled by an MPC speed tracking controller that requested a battery power P_k [58]. At each time k, P_k is then converted to the requested current by solving the quadratic equation as documented in [59]. Note that in this case, the preview of i_k is assumed to be unavailable, i.e., $\delta i_{k+j} = 0$ throughout the entire prediction horizon. Due to the recent advancement of connected and automated vehicle, the preview of P_k may be estimated with acceptable accuracy. However, such availability assumption can be too restrictive for the present study.

TABLE I VARIATION OF ECM PARAMETERS

-	Cell 1	Cell 2	Cell 3	Cell 4	Cell 5
C^n	1.0141	0.9677	1.0744	0.9150	0.9945
R_o^n	1.0640	0.9043	1.0088	1.0818	1.0907
R_p^n	1.0341	1.0111	1.0563	0.9016	1.0643
C_n^n	1.0678	0.9226	0.9325	0.9712	1.0911

For each of these two scenarios, the three MPC strategies are simulated. Recall that the first MPC (denoted as J_t) tracks all cell voltages to follow the same reference trajectory generated by a nominal cell. The second MPC (denoted as $J_{\rm m}$) maximizes the lowest cell voltage. And the third MPC (denoted as J_{Δ}) minimizes the difference between the highest and lowest cell voltages. For all setups, N = 5 is used and all cells are initialized to be fully charged, i.e., with $s_0^n = 1$. The cell parameters C^n , R_o^n , R_p^n , and C_p^n are randomly generated to be within 10% deviation from the nominal values. In other words, Let C^0 , R_o^0 , R_p^0 , and C_p^0 be the nominal values as depicted in Fig. 3. Then Table I lists the ratio between C^n , R_o^n , R_p^n , and C_p^n with respect to their nominal values. Finally, sampling time T_s is chosen to be 1 second, and the bound constraints on the balancing currents are set to be $u_{\min} = -2A$ and $u_{\text{max}} = 2A$. Recall that a weighting matrix R is imposed in the cost functions (10a), (11a) and (13a) to balance control performance and control efforts by penalizing large balancing currents. It is intuitive to see that if R = 0, MPC can choose however large balancing currents so that all cells voltages are balanced. However, this may result in energy waste due to Ohmic loss in balancing circuits. On the other hand, when R is large, MPC will simply set all balancing current to 0, resulting in poor control performance. In this paper, the value for R is manually tuned to that a desired balance between control performance and control efforts is achieved.

A. Steady-State Condition

In this scenario, constant commanded current i_k is used to represent the steady-state operation. Without active cell balancing, the battery pack can last 1,527 seconds until the lowest cell voltage drops below v_{\min} . For MPCs with prediction horizon p = 5, J_t can extend the operation time to 1,599 seconds (4.72% increase), $J_{\rm m}$ extends to 1,640 seconds (7.40% increase), while J_{Δ} extends to 1,682 seconds (6.61% increase). This is summarized in Table II and Figs. 5, 6 and 7, where each cell's voltage, SOC, and balancing current are plotted. It can be seen that the balancing currents for three MPC strategies possess a similar pattern, and are near constant or vary slowly for most of the time. Note that the capacities of cells in our simulation range from 11.18 Ah to 13.41 Ah. If the battery cells are allowed to operate until SOC reaches 0, then with $u_{\text{max}} = 2A$ roughly 8.94% of range extension is possible. However, since the cell voltage is not allowed to drop below y_{min} , the battery operations terminate before SOC reaches 0 for all simulations. In addition, the voltage is a nonlinear function of the SOC, especially around the low SOC area, which explains the lower extension reported in Table II.

TABLE II
SIMULATION RESULTS FOR CONSTANT DISCHARGE CURRENT

Setup	Operation Time [s]	Extension
No balancing	1,527	-
J_{t}	1,599	4.72%
$J_{ m m}$	1,640	7.40%
J_{Δ}	1,628	6.61%

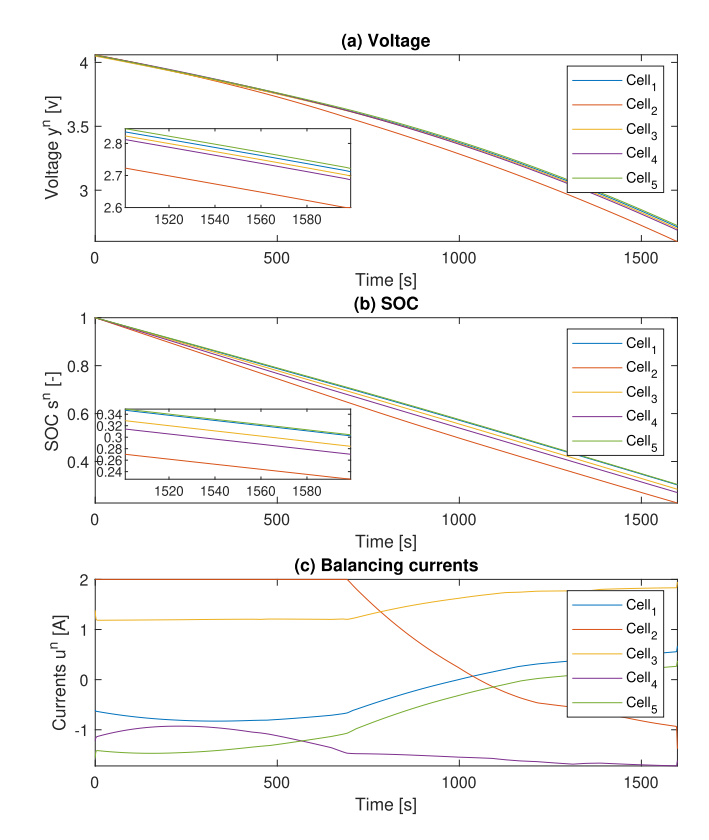


Fig. 5. Results for J_t with constant discharge current.

Furthermore, Fig. 8 compares the lowest cell voltage for different control strategies, as well as the balancing effort, which represents an index for Ohmic heating loss due to balancing and is calculated as

$$e_k = u_k^T u_k$$
.

It is clear from Fig. 8(b) that, $J_{\rm t}$ requires larger balancing efforts, especially when the SOC and voltage are still high. This is because $J_{\rm t}$ tracks all cell voltages to the nominal trajectory, and hence will try to balance even when all cell voltages are clearly away from the minimum bound $v_{\rm min}$. When the cell voltage gets closer to $v_{\rm min}$, all three MPCs utilize a similar amount of balancing efforts, while J_{Δ} is a little more aggressive.

Note that in practice, p is chosen in a way to balance control performance and prediction horizon. When p is small, MPC relies on shorter prediction to make control decision, and often can be short-sighted. When p is large, MPC could make better control decision, but at the same time the required computation can be much higher that prevents real-time implementation. See Section V-C for discussion on the relationship between prediction horizon p and computation

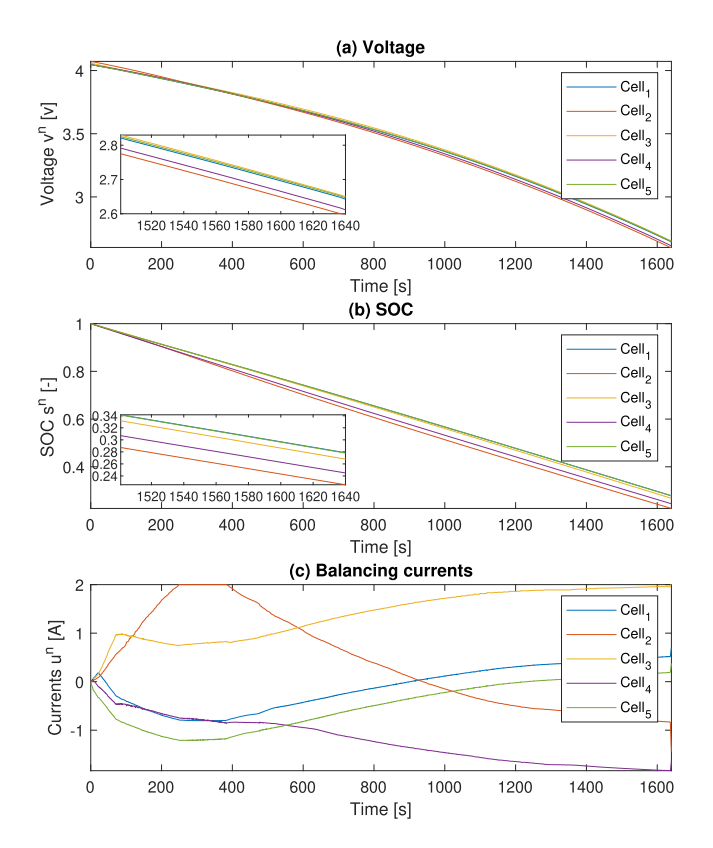


Fig. 6. Results for $J_{\rm m}$ with constant discharge current.

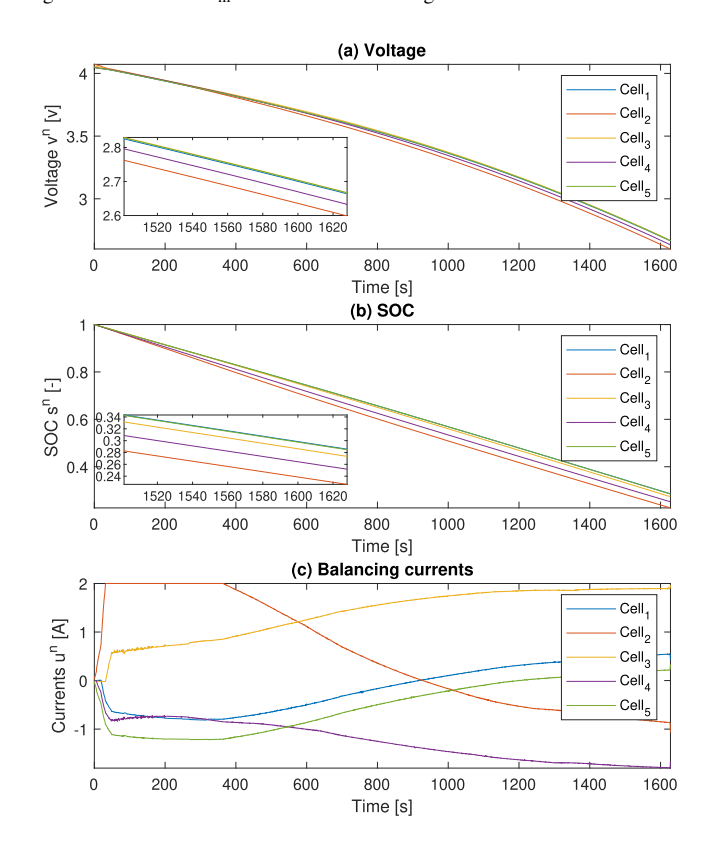


Fig. 7. Results for J_{Δ} with constant discharge current.

time. Furthermore, when prediction horizon is too long, it can also result in degraded control performance due to model inaccuracy, dynamic load profile, etc. In this section, p is

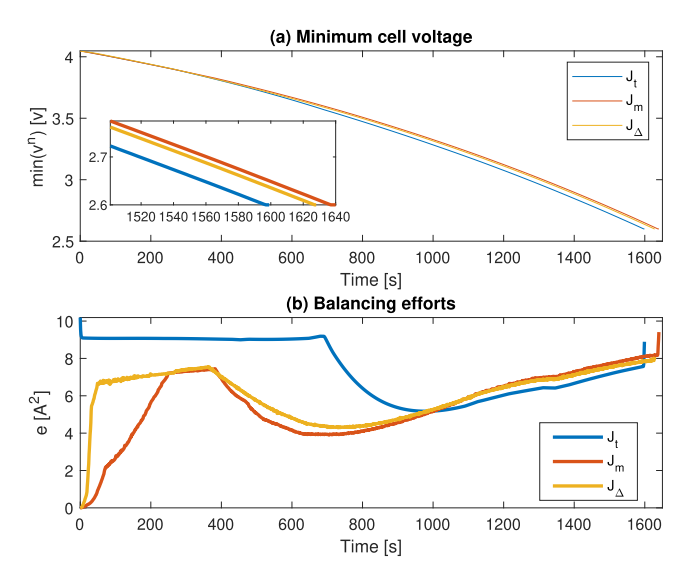


Fig. 8. Comparison of the lowest cell voltages and balancing efforts for different MPC-based balancing control strategies with constant discharge current

manually selected to achieve best control performance with a manageable computation time. Furthermore, to see the impact of prediction horizon, we set p=35, reduce the current to a reasonable level, and at the same time divide R by 7 to balance the two terms in the cost functions. For J_t formulation, without balancing, the battery terminated at 5 hours, 16 minutes and 45 seconds, while with active cell balancing, it terminated at 5 hours, 33 minutes and 52 seconds, providing a 5.13% range extension, which is a bit more than the 4.72% reported in Table II. Note that conducting a similar simulation for J_m and J_Δ is not possible due to the long simulation time (see Table IV).

B. Dynamic Condition

In this section, the vehicle follows a realistic driving cycle, i.e., FTP cycle, where the vehicle is controlled by an MPC speed tracking controller, as presented in [58]. The vehicle speed profile and corresponding requested power of FTP cycle is shown in Fig. 9, which is then concatenated and scaled up so to provide a realistic assessment of the range extension within a manageable amount of simulation time. In particular, over 3 hours and 20 minutes are simulated to mimic actual driving scenarios.

The range extensions for different controllers for p = 5, 10, 15, together with their balancing efforts defined as $e = \frac{1}{K} \sum_{k=1}^{K} e_k$ where K is the length of battery operation, are presented in Tables III. With prediction horizon p = 5, all control strategies can achieve 9.33% of driving range extension, with very minimum balancing efforts. However, the driving range extensions slightly decrease with the increase of p. Such slight decrease may be due to the fact that we are not using preview on load profile in the present simulation, making longer prediction horizon less effective.

Finally, Fig. 10 plots the cell voltages for all strategies, where very similar behaviors are observed. Fig. 11 compares the lowest cell voltages and balancing efforts for a short period of time that is preceding to the pack failure. Though the lowest

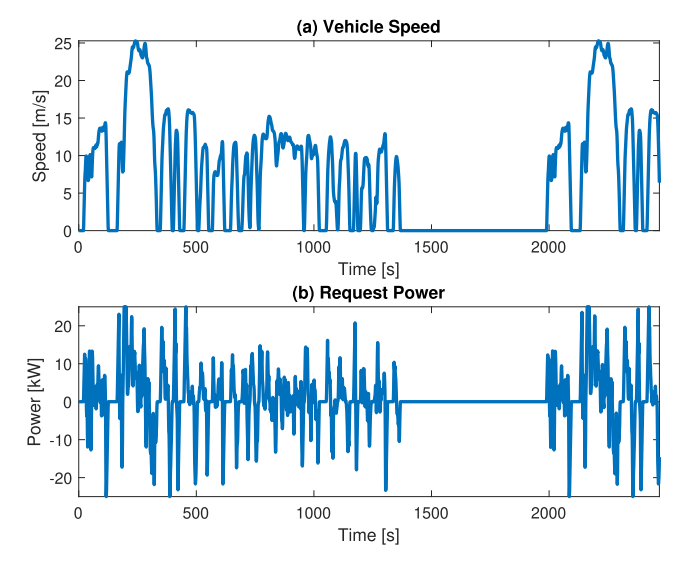


Fig. 9. Speed profile and corresponding requested power of FTP driving cycle.

TABLE III
SIMULATION RESULTS FOR FTP CYCLE

Setup	p	Distance [m]	Extension	$e [A^2]$
No balancing	-	110949.0	-	-
J_{t}	5	121297.7	9.33%	3.8
$J_{ m m}$	5	121297.7	9.33%	0.4
J_{Δ}	5	121297.7	9.33%	0.36
J_{t}	10	121297.7	9.33%	15.51
J_{m}	10	121297.7	9.33%	0.87
J_{Δ}	10	120036.13	8.19%	2.7
J_{t}	15	120036.13	8.19%	15.71
$J_{ m m}$	15	119515.93	7.72%	8.61
J_{Δ}	15	120036.13	8.19	11.68

TABLE IV

COMPARISON OF COMPUTATIONAL TIME (IN MILLISECOND)

\overline{p}	5	15	25	35
J_{t}	4.3	11.23	16.47	28.83
$J_{ m m}$	3.35	780.32	719.10	701.36
J_{Λ}	8.34	2507.43	2128.6	5309.3

cell voltages for three control strategies are almost the same in Fig. 11(a), the balancing efforts are very much different. In particular, similar to the steady-state scenario, J_t requires the maximum amount of balancing efforts.

C. Further Discussion and Future Direction

The computational time required by each MPC are summarized in Table IV, which is measured on a desktop computer with standard CPU using Matlab's standard matrix operations and quadprog as the QP solver. As can be seen, J_t is always manageable even for longer prediction horizon, while J_m and J_Δ are applicable for real time implementation only when p is smaller than 15.

From Table II, it can be seen that for steady-state condition, $J_{\rm m}$ and J_{Δ} can achieve better driving range extensions with lower balancing efforts. However, they require a significant amount of computation time compared to $J_{\rm t}$, according to

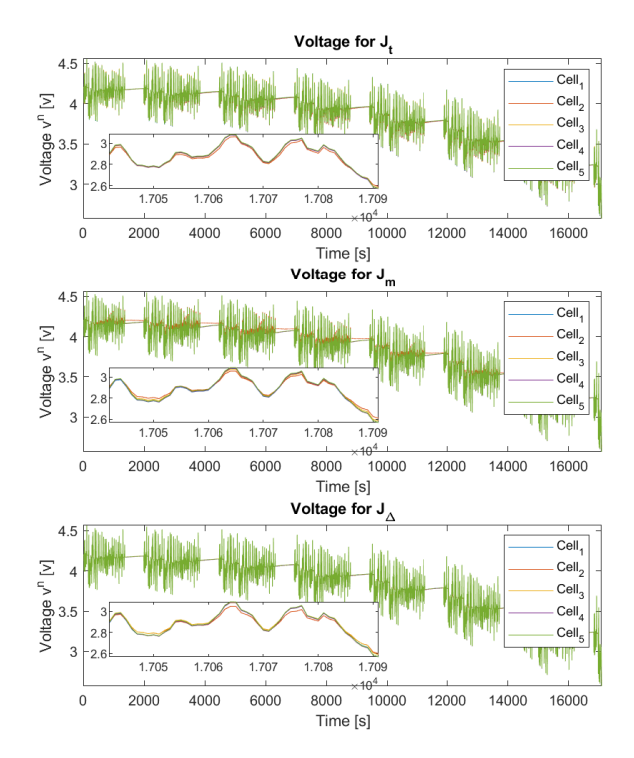


Fig. 10. Comparison of cell voltages for different MPC-based balancing control strategies with FTP cycle.

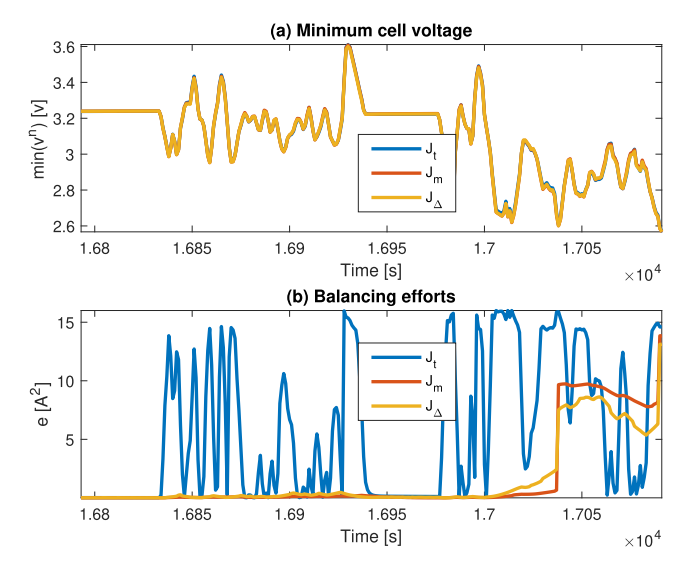


Fig. 11. Comparison of the lowest voltages and balancing efforts for different MPC-based balancing control strategies with FTP cycle.

Table IV. In particular, the high computation required by J_{Δ} with long prediction horizon may prevent its real-time implementation in embedded devices. Therefore, with shorter prediction horizon only, they seem to be better choices for steady-state condition. On the other hand, according to Table III, for transient condition, $J_{\rm t}$ is much more robust against disturbance on future load profile, achieves better range extension with a slightly higher balancing efforts. Therefore, $J_{\rm t}$ seems to be a better choice for the transient condition.

These findings suggest that a hybrid approach may provide best driving range extension in reality that has a mix of both steady-state and transient condition. In other words, a steady state detection algorithm [60] can be implemented to determine whether the vehicle speed is at steady-state condition. Based on the current driving condition (steady-state v.s. transient), a switching MPC can then be constructed to switch between $J_{\rm m}/J_{\Delta}$ for steady-state condition and $J_{\rm t}$ for transient condition. To avoid chattering, hysteresis can also be introduced.

Note that in our work, we assume the same OCV v.s. SOC curve as shown in Fig. 4 holds for all cells, and only consider cell to cell variations on C^n , R_o^n , R_p^n , and C_p^n . In reality, the OCV v.s SOC curves can be different for different cells, especially during highly dynamic conditions. Such discrepancy may decrease balancing efficiency, making the range extension lower than the 7%-9% as reported by our simulation environment. One possible solution is to modify (10a), (11a), (13a) to include both voltage and SOC terms, with a price of complexity increase. Note also that only 5 connected cells are considered in this paper. In reality, EV batteries usually consist of hundreds of cells. To scale up the proposed MPC strategies, several approaches can be considered. First, distributed and hierarchical control approach [41], [42] can be used so that each MPC agent solves a relatively smaller optimization problem. Second, explicit MPC approach [61] can be used to reduce online computation while maintaining same real-time control performance. Investigating these approaches are reserved as future work. Recall that one of the sources of cell variations is aging, which can also lead to model mismatch. In this regard, parameter estimation has been studied in the literature [62] to estimate ECM parameters in real time, which is then used for adaptive control design. In the future, we will also investigate the impact of model mismatch and parameter estimation algorithms that can be utilized for real-time compensation.

Finally, battery cell balancing has been studied outside of EV applications. See for example [40]. The proposed MPC strategies can be straightforwardly extended to non-EV applications, since the proposed methodology, as discussed in Section IV, are formulated based on generic battery ECM modeling. It is worth noting that the input constraints u_{\min} and u_{\max} , minimum voltage v_{\min} , as well as objective function calibration R need to be tuned based on applications. It is also envisioned that the proposed methodology can find several applications such as renewable energy integration and EV fleet control, where efficient operations of batteries is a key enabler.

VI. CONCLUSION

In this paper, we studied the active battery cell balancing problem by using model predictive control (MPC) for electric vehicle driving range extension. Specifically, three MPC strategies were investigated. In the first control strategy, a nominal cell was used to compute a short term reference trajectory and MPC was set to track all cell voltages to follow this reference trajectory. In the second and third control strategies, MPC was set to maximize the lowest voltage cell and to minimize the difference between the highest and lowest cell voltage, respectively. To demonstrate the effectiveness of the proposed control strategies, both steady-state and transient conditions were simulated. In general, a 7% driving range extension can

be achieved for steady-state condition and 9% for transient condition. It was also found that different driving scenarios may favor different control strategy, and a hybrid approach might be needed. Compared to the existing approaches in literature, our approach can achieve similar driving range extension without restrictively requiring the trip duration to be known in advance. For future work, we would focus on (1) designing an observer to estimate the cells' voltage and SOC, as full state feedback was assumed in the current work, (2) developing control algorithms to handle series-parallel connections, (3) scaling up the algorithms for a large number of connected cells, and (4) hardware validation of the proposed MPC strategies.

REFERENCES

- [1] Electric Vehicles Projected to Make Up 31% of the Global Fleet by 2050. Accessed: Jul. 16, 2022. [Online]. Available: https://electrek.co/2021/10/26/electric-vehicles-projected-to-make-up-31-of-the-global-fleet-by-2050/
- [2] U.S. Department of Energy, Alternative Fuels Data Center. Emissions From Electric Vehicles. Accessed: Jul. 16, 2022. [Online]. Available: https://afdc.energy.gov/vehicles/electric_emissions.html
- [3] X. Hu, H. Yuan, C. Zou, Z. Li, and L. Zhang, "Co-estimation of state of charge and state of health for lithium-ion batteries based on fractional-order calculus," *IEEE Trans. Veh. Technol.*, vol. 67, no. 11, pp. 10319–10329, Nov. 2018.
- [4] Q. Wang, Z. Wang, L. Zhang, P. Liu, and Z. Zhang, "A novel consistency evaluation method for series-connected battery systems based on realworld operation data," *IEEE Trans. Transport. Electrific.*, vol. 7, no. 2, pp. 437–451, Jun. 2021.
- [5] M. Dubarry, N. Vuillaume, and B. Y. Liaw, "Origins and accommodation of cell variations in Li-ion battery pack modeling," *Int. J. Energy Res.*, vol. 34, no. 2, pp. 216–231, Feb. 2010.
- [6] R. de Castro, H. Pereira, R. E. Araújo, J. V. Barreras, and H. C. Pangborn, "qTSL: A multilayer control framework for managing capacity, temperature, stress, and losses in hybrid balancing systems," IEEE Trans. Control Syst. Technol., vol. 30, no. 3, pp. 1228–1243, May 2022.
- [7] F. S. J. Hoekstra, H. J. Bergveld, and M. C. F. Donkers, "Range maximisation of electric vehicles through active cell balancing using reachability analysis," in *Proc. Amer. Control Conf. (ACC)*, Philadelphia, PA, USA, Jul. 2019, pp. 1567–1572.
- [8] F. S. J. Hoekstra, L. A. W. Ribelles, H. J. Bergveld, and M. C. F. Donkers, "Real-time range maximisation of electric vehicles through active cell balancing using model-predictive control," in *Proc. Amer. Control Conf. (ACC)*, Denver, CO, USA, Jul. 2020, pp. 2219–2224.
- [9] K. Smith, E. Wood, S. Santhanagopalan, G. Kim, and A. Pesaran, "Advanced models and controls for prediction and extension of battery lifetime (presentation)," Nat. Renew. Energy Lab. (NREL), Golden, CO, USA, Tech. Rep. NREL/PR-5400-61037, Feb. 2014. [Online]. Available: https://www.osti.gov/biblio/1114881
- [10] M. Einhorn, W. Roessler, and J. Fleig, "Improved performance of serially connected Li-ion batteries with active cell balancing in electric vehicles," *IEEE Trans. Veh. Technol.*, vol. 60, no. 6, pp. 2448–2457, Jul. 2011.
- [11] M. Daowd, N. Omar, P. Van Den Bossche, and J. Van Mierlo, "Passive and active battery balancing comparison based on MATLAB simulation," in *Proc. IEEE Vehicle Power Propuls. Conf.*, Sep. 2011, pp. 1–7.
- [12] F. Mestrallet, L. Kerachev, J. Crebier, and A. Collet, "Multiphase interleaved converter for lithium battery active balancing," *IEEE Trans. Power Electron.*, vol. 29, no. 6, pp. 2874–2881, Jun. 2014.
- [13] L. Maharjan, S. Inoue, H. Akagi, and J. Asakura, "State-of-charge (SOC)-balancing control of a battery energy storage system based on a cascade PWM converter," *IEEE Trans. Power Electron.*, vol. 24, no. 6, pp. 1628–1636, Jun. 2009.
- [14] S. Li, C. C. Mi, and M. Zhang, "A high-efficiency active battery-balancing circuit using multiwinding transformer," *IEEE Trans. Ind. Appl.*, vol. 49, no. 1, pp. 198–207, Jan. 2013.
- [15] Y. Shang, B. Xia, C. Zhang, N. Cui, J. Yang, and C. C. Mi, "An automatic equalizer based on forward–flyback converter for seriesconnected battery strings," *IEEE Trans. Ind. Electron.*, vol. 64, no. 7, pp. 5380–5391, Jul. 2017.

- [16] Y. Shang, N. Cui, and C. Zhang, "An optimized any-cell-to-any-cell equalizer based on coupled half-bridge converters for series-connected battery strings," *IEEE Trans. Power Electron.*, vol. 34, no. 9, pp. 8831–8841, Sep. 2019.
- [17] C. Pinto, J. V. Barreras, E. Schaltz, and R. E. Araújo, "Evaluation of advanced control for Li-ion battery balancing systems using convex optimization," *IEEE Trans. Sustain. Energy*, vol. 7, no. 4, pp. 1703–1717, Oct. 2016.
- [18] M. Preindl, "A battery balancing auxiliary power module with predictive control for electrified transportation," *IEEE Trans. Ind. Electron.*, vol. 65, no. 8, pp. 6552–6559, Aug. 2018.
- [19] R. D. Anderson, R. Zane, G. Plett, D. Maksimovic, K. Smith, and M. S. Trimboli, "Life balancing—A better way to balance large batteries," SAE Tech. Paper 2017-01-1210, 2017.
- [20] L. Y. Wang et al., "Balanced control strategies for interconnected heterogeneous battery systems," *IEEE Trans. Sustain. Energy*, vol. 7, no. 1, pp. 189–199, Jan. 2016.
- [21] M. Evzelman, M. M. U. Rehman, K. Hathaway, R. Zane, D. Costinett, and D. Maksimovic, "Active balancing system for electric vehicles with incorporated low-voltage bus," *IEEE Trans. Power Electron.*, vol. 31, no. 11, pp. 7887–7895, Nov. 2016.
- [22] J. Xu, B. Cao, S. Li, B. Wang, and B. Ning, "A hybrid criterion based balancing strategy for battery energy storage systems," *Proc. Energy*, vol. 103, pp. 225–230, Dec. 2016.
- [23] Z. C. Gao, C. S. Chin, W. D. Toh, J. Chiew, and J. Jia, "State-of-charge estimation and active cell pack balancing design of lithium battery power system for smart electric vehicle," *J. Adv. Transp.*, vol. 2017, Nov. 2017, Art. no. 6510747.
- [24] S. Narayanaswamy, S. Park, S. Steinhorst, and S. Chakraborty, "Multi-pattern active cell balancing architecture and equalization strategy for battery packs," in *Proc. Int. Symp. Low Power Electron. Design*, Seattle, WA, USA, Jul. 2018, pp. 1–6.
- [25] M. Kauer, S. Narayanaswamy, S. Steinhorst, M. Lukasiewycz, and S. Chakraborty, "Many-to-many active cell balancing strategy design," in *Proc. 20th Asia South Pacific Design Autom. Conf.*, Chiba, Japan, Jan. 2015, pp. 267–272.
- [26] D. Liao-McPherson, M. M. Nicotra, A. L. Dontchev, I. V. Kolmanovsky, and V. M. Veliov, "Sensitivity-based warmstarting for nonlinear model predictive control with polyhedral state and control constraints," *IEEE Trans. Autom. Control*, vol. 65, no. 10, pp. 4288–4294, Oct. 2020.
- [27] S. D. Cairano, D. Bernardini, A. Bemporad, and I. V. Kolmanovsky, "Stochastic MPC with learning for driver-predictive vehicle control and its application to HEV energy management," *IEEE Trans. Control Syst. Technol.*, vol. 22, no. 3, pp. 1018–1031, May 2014.
- [28] D. Q. Mayne, J. B. Rawlings, C. V. Rao, and P. O. M. Scokaert, "Constrained model predictive control: Stability and optimality," *Automatica*, vol. 36, no. 6, pp. 789–814, Jun. 2000.
- [29] Y. Shi, H. D. Tuan, A. V. Savkin, T. Q. Duong, and H. V. Poor, "Model predictive control for smart grids with multiple electric-vehicle charging stations," *IEEE Trans. Smart Grid*, vol. 10, no. 2, pp. 2127–2136, Mar. 2019.
- [30] D. Q. Mayne, M. M. Seron, and S. V. Raković, "Robust model predictive control of constrained linear systems with bounded disturbances," *Automatica*, vol. 41, no. 2, pp. 219–224, Feb. 2005.
- [31] H. Chen and F. Allgöwer, "A quasi-infinite horizon nonlinear model predictive control scheme with guaranteed stability," *Automatica*, vol. 34, no. 10, pp. 1205–1217, 1998.
- [32] T. Besselmann, J. Lofberg, and M. Morari, "Explicit MPC for LPV systems: Stability and optimality," *IEEE Trans. Autom. Control*, vol. 57, no. 9, pp. 2322–2332, Sep. 2012.
- [33] L. McCurlie, M. Preindl, and A. Emadi, "Fast model predictive control for redistributive lithium-ion battery balancing," *IEEE Trans. Ind. Electron.*, vol. 64, no. 2, pp. 1350–1357, Feb. 2017.
- [34] F. Altaf, B. Egardt, and L. J. Mårdh, "Load management of modular battery using model predictive control: Thermal and state-of-charge balancing," *IEEE Trans. Control Syst. Technol.*, vol. 25, no. 1, pp. 47–62, Jan. 2017.
- [35] L. Zheng, J. Zhu, G. Wang, D. D.-C. Lu, P. McLean, and T. He, "Model predictive control based balancing strategy for series-connected lithiumion battery packs," in *Proc. 19th Eur. Conf. Power Electron. Appl. (EPE ECCE Europe)*, Sep. 2017, pp. P.1–P.8.
- [36] J. Liu, Y. Chen, and H. K. Fathy, "Nonlinear model-predictive optimal control of an active cell-to-cell lithium-ion battery pack balancing circuit," *IFAC-PapersOnLine*, vol. 50, no. 1, pp. 14483–14488, Jul. 2017.
- [37] M. F. Samadi and M. Saif, "Nonlinear model predictive control for cell balancing in Li-ion battery packs," in *Proc. Amer. Control Conf.*, Jun. 2014, pp. 2924–2929.

- [38] A. Pozzi, M. Zambelli, A. Ferrara, and D. M. Raimondo, "Balancing-aware charging strategy for series-connected lithium-ion cells: A nonlinear model predictive control approach," *IEEE Trans. Control Syst. Technol.*, vol. 28, no. 5, pp. 1862–1877, Sep. 2020.
- [39] S. M. Salamati, S. A. Salamati, M. Mahoor, and F. R. Salmasi, "Leveraging adaptive model predictive controller for active cell balancing in Li-ion battery," in *Proc. North Amer. Power Symp. (NAPS)*, Sep. 2017, pp. 1–6.
- [40] T. Morstyn, M. Momayyezan, B. Hredzak, and V. G. Agelidis, "Distributed control for state-of-charge balancing between the modules of a reconfigurable battery energy storage system," *IEEE Trans. Power Electron.*, vol. 31, no. 11, pp. 7986–7995, Nov. 2016.
- [41] X. Kong, X. Liu, L. Ma, and K. Y. Lee, "Hierarchical distributed model predictive control of standalone wind/solar/battery power system," *IEEE Trans. Syst., Man, Cybern. Syst.*, vol. 49, no. 8, pp. 1570–1581, Aug. 2019.
- [42] Z. Gong et al., "Distributed control of active cell balancing and low-voltage bus regulation in electric vehicles using hierarchical modelpredictive control," *IEEE Trans. Ind. Electron.*, vol. 67, no. 12, pp. 10464–10473, Dec. 2020.
- [43] A. Nawaz, J. Wu, J. Ye, Y. Dong, and C. Long, "Distributed MPC-based energy scheduling for islanded multi-microgrid considering battery degradation and cyclic life deterioration," *Appl. Energy*, vol. 329, Jan. 2023, Art. no. 120168.
- [44] H. Fang, D. Wu, and T. Yang, "Cooperative management of a lithium-ion battery energy storage network: A distributed MPC approach," in *Proc. IEEE 55th Conf. Decis. Control (CDC)*, Dec. 2016, pp. 4226–4232.
- [45] J. Chen, A. Behal, and C. Li, "Active cell balancing by model predictive control for real time range extension," in *Proc. 60th IEEE Conf. Decis. Control (CDC)*, Austin, TX, USA, Dec. 2021, pp. 271–276, doi: 10.1109/CDC45484.2021.9682869.
- [46] Z. Pei, X. Zhao, H. Yuan, Z. Peng, and L. Wu, "An equivalent circuit model for lithium battery of electric vehicle considering self-healing characteristic," *J. Control Sci. Eng.*, vol. 2018, pp. 1–11, Jun. 2018.
- [47] S. Madani, E. Schaltz, and S. K. Kær, "An electrical equivalent circuit model of a lithium titanate oxide battery," *Batteries*, vol. 5, no. 1, p. 31, Mar. 2019.
- [48] B. Y. Liaw, R. G. Jungst, A. Urbina, and T. L. Paez, "Modeling of battery life I. The equivalent circuit model (ECM) approach," Sandia Nat. Lab., Livermore, CA, USA, Tech. Rep., 2023. [Online]. Available: http://www.sandia.gov/ess/EESAT/2003_papers/Liaw.pdf
- [49] H. He, R. Xiong, X. Zhang, F. Sun, and J. Fan, "State-of-charge estimation of the lithium-ion battery using an adaptive extended Kalman filter based on an improved Thevenin model," *IEEE Trans. Veh. Technol.*, vol. 60, no. 4, pp. 1461–1469, May 2011.
- [50] J. Wehbe and N. Karami, "Battery equivalent circuits and brief summary of components value determination of lithium ion: A review," in *Proc.* 3rd Int. Conf. Technol. Adv. Electr., Electron. Comput. Eng. (TAEECE), Beirut, Lebanon, Apr. 2015, pp. 45–49.
- [51] M. Dubarry, V. Svoboda, R. Hwu, and B. Y. Liaw, "A roadmap to understand battery performance in electric and hybrid vehicle operation," *J. Power Sources*, vol. 174, no. 2, pp. 366–372, Dec. 2007.
- [52] X. Lin et al., "A lumped-parameter electro-thermal model for cylindrical batteries," J. Power Sources, vol. 257, pp. 1–11, Jul. 2014.
- [53] R. de Castro, C. Pinto, J. V. Barreras, R. E. Araújo, and D. A. Howey, "Smart and hybrid balancing system: Design, modeling, and experimental demonstration," *IEEE Trans. Veh. Technol.*, vol. 68, no. 12, pp. 11449–11461, Dec. 2019.
- [54] A. Alessio and A. Bemporad, "A survey on explicit model predictive control," in *Nonlinear Model Predictive Control*. Berlin, Germany: Springer, 2009, pp. 345–369.
- [55] A. Bemporad, D. Bernardini, R. Long, and J. Verdejo, "Model predictive control of turbocharged gasoline engines for mass production," SAE Tech. Paper 2018-01-0875, 2018.
- [56] A. Bemporad, D. Bernardini, M. Livshiz, and B. Pattipati, "Supervisory model predictive control of a powertrain with a continuously variable transmission," SAE Tech. Paper 2018-01-0860, 2018.
- [57] J. Nocedal and S. Wright, *Numerical Optimization*. New York, NY, USA: Springer, 2006.
- [58] J. Chen, M. Liang, and X. Ma, "Probabilistic analysis of electric vehicle energy consumption using MPC speed control and nonlinear battery model," in *Proc. IEEE Green Technol. Conf. (GreenTech)*, Denver, CO, USA, Apr. 2021, pp. 181–186.
- [59] Y. Kim, S. Mohan, J. B. Siegel, and A. G. Stefanopoulou, "Maximum power estimation of lithium-ion batteries accounting for thermal and electrical constraints," in *Proc. ASME Dyn. Syst. Control Conf.*, 2013, pp. 1–8.

- [60] J. Wu, Y. Chen, S. Zhou, and X. Li, "Online steady-state detection for process control using multiple change-point models and particle filters," *IEEE Trans. Autom. Sci. Eng.*, vol. 13, no. 2, pp. 688–700, Apr. 2016.
- [61] A. Bemporad, M. Morari, V. Dua, and E. N. Pistikopoulos, "The explicit linear quadratic regulator for constrained systems," *Automatica*, vol. 38, no. 1, pp. 3–20, Jan. 2002.
- [62] F. Guo, G. Hu, S. Xiang, P. Zhou, R. Hong, and N. Xiong, "A multi-scale parameter adaptive method for state of charge and parameter estimation of lithium-ion batteries using dual Kalman filters," *Energy*, vol. 178, pp. 79–88, Jul. 2019.



Jun Chen (Senior Member, IEEE) received the bachelor's degree in automation from Zhejiang University, Hangzhou, China, in 2009, and the Ph.D. degree in electrical engineering from Iowa State University, Ames, IA, USA, in 2014. He is currently an Assistant Professor with the ECE Department, Oakland University. His research interests include artificial intelligence and optimal control, with applications in intelligent vehicles and energy systems. He is a member of SAE. He was a recipient of the NSF CAREER Award, the Best Paper Award from

IEEE TRANSACTIONS ON AUTOMATION SCIENCE AND ENGINEERING, the Best Paper Award from IEEE INTERNATIONAL CONFERENCE ON ELECTRO INFORMATION TECHNOLOGY, the Faculty Recognition Award for Research from Oakland University, the Publication Achievement Award from the Idaho National Laboratory, the Research Excellence Award from Iowa State University, and the Outstanding Student Award from Zhejiang University.



Zhaojian Li (Senior Member, IEEE) received the bachelor's degree from the Department of Civil Aviation, Nanjing University of Aeronautics and Astronautics, China, and the M.S. and Ph.D. degrees in aerospace engineering (flight dynamics and control) from the University of Michigan, Ann Arbor, in 2013 and 2015, respectively. He was an Algorithm Engineer with General Motors, from January 2016 to July 2017. He is an Assistant Professor with the Department of Mechanical Engineering, Michigan State University. He is the author of more than 40 top

journal articles and several patents. His research interests include learning-based control, nonlinear and complex systems, and robotics and automated vehicles. He was a recipient of the NSF CAREER Award. He is an Associate Editor of journal of *Evolving Systems*, American Control Conference, and ASME Dynamics and Control Conference.



Aman Behal (Senior Member, IEEE) received the integrated M.Tech. degree in EE from IIT Bombay, Mumbai, India, in 1996, and the Ph.D. degree in controls and robotics from Clemson University, Clemson, SC, USA, in 2001. After a brief stint as a Post-Doctoral Associate in Bioengineering with Clemson University, he joined as a Faculty Member of the Department of Electrical and Computer Engineering, Clarkson University, Potsdam, NY, USA, in 2003. In 2006, he joined the University of Central Florida, Orlando, FL, USA, where he is currently a

Professor jointly with the Department of Electrical and Computer Engineering and the NanoScience Technology Center. His current research interests include assistive robotics and nonlinear controls. He was an Associate Editor of the IEEE TRANSACTIONS ON CYBERNETICS. He is an Associate Editor on the Editorial Board of the IEEE TRANSACTIONS ON CONTROL SYSTEMS TECHNOLOGY.



Chong Li (Senior Member, IEEE) is an Adjunct Associate Professor with the Department of Electrical Engineering, Columbia University, New York; and the Founder and a CEO of the decentralized data cloud company "Oort." He was with Qualcomm Research on 4G LTE and 5G systems design. He is a holder of more than 200 international/U.S. patents. He is the author of the book *Reinforcement Learning for Cyber-Physical Systems* (Taylor & Francis CRC Press). His research interests include information theory, machine learning, distributed database, com-

puting systems (e.g., blockchain), networked control and communication, and PYH/MAC systems design for advance telecommunication technologies (5G and beyond). He is a Grant Review Committee Member of the Natural Sciences and Engineering Research Council of Canada. He is also the President of the Science and Technology Economic Committee at China–U.S. Chamber of Commerce.